

Article

The Push-Over Test and Numerical Analysis Study on the Mechanical Behavior of the GFRP Frame for Sustainable Prefabricated Houses

Yeou-Fong Li *, Jian-Yu Lai and Chung-Cheng Yu

Department of Civil Engineering, National Taipei University of Technology, Taipei 10608, Taiwan; ferrari78316@yahoo.com.tw (J.-Y.L.); jkui78@yahoo.com.tw (C.-C.Y.)

* Correspondence: yfli@ntut.edu.tw

Received: 25 September 2019; Accepted: 25 November 2019; Published: 28 November 2019



Abstract: The glass fiber reinforced plastics (GFRP) composite material is a low carbon emission, low life cycle cost, and sustainable material. In this paper, the structural behavior of the lateral force resistant performance of GFRP composite material frames with steel joints was presented, and the energy dissipation and failure modes of the GFRP frames were discussed. A total of six GFRP frames, including single-span and double-span frames with and without diagonal bracing members, were tested by pushover tests to obtain the lateral load-displacement relationships of the GFRP frames. The force-displacement relationship and the energy dissipation of the GFRP frames were examined in the pushover test. In addition, the numerical analysis was performed to obtain the lateral load-displacement relationships of the GFRP frames under pushover tests. When the numerical analysis results and the experimental results were compared, the absolute average errors of the maximum loads were less than 4%, and the lateral load-displacement relationships were close to each other. The numerical analysis results can predict the experimental force-displacement relationships of the GFRP frames.

Keywords: glass fiber reinforced plastics; frame; pushover test; low carbon emission; low life cycle cost; sustainable

1. Introduction

Recently, extreme weather has severely affected rainfall patterns and increased the incidents of flooding and other meteorological disasters, which inundated villages and cities and led to the destruction of properties. Prefabricated residential buildings have an advantage in quick installation to become a temporary residence for post-disaster relief of refugees. Prefabricated houses can also be used in coastal areas as vacation homes and other similar purposes with a minimal impact on the environment.

Concrete material has been identified as a major contributor to the greenhouse gas carbon dioxide in the atmosphere. Steel prefabricated houses and wooden houses are both easily corroded and have costly maintenance problems.

As an alternative, fiber reinforced plastic (FRP) composite material has been widely used in the retrofit and repair of buildings and bridges due to its merits of anti-corrosion, light-weight, high strength-to-weight ratio, high elastic modulus, high durability, easy-to-assemble, and great design flexibility. Recently, the FRP composite material was widely used in sporting goods, automotive, aerospace, and civil engineering. FRP composite material can also offer low maintenance cost, low life-cycle cost, and low carbon dioxide emission [1]. From the research results by Li et al. [1], the research results show that the total carbon dioxide emission of the GFRP in various stages (production,

transportation, and construction stages) is significantly lower than traditional reinforced concrete (RC) and steel pedestrian bridges, which makes GFRP material environmentally friendly. Fabric-reinforced cementitious matrix (FRCM) composites and FRP composite bars as structural members can significantly enhance structural safety and sustainability in the construction industry [2–4].

Furthermore, FRP composite materials can be recycled and reused [5,6]. Therefore, FRP is a sustainable material for civil engineering usage. Because of the aforementioned advantages, the FRP composite materials can be used for prefabricated houses in mountainous or coastal areas without the worries of being affected by corrosion brought by the harsh environments.

FRP composite material has been used in civil engineering since the 1980s [7]. The experimental strength tests, such as fatigue and bending tests, and the finite-element analysis were performed on the GFRP composite bridge deck [8–14]. The structural behaviors of different sections of GFRP members were investigated, and the results showed that GFRP structural members could be applied to civil engineering [15–17]. The mechanical behavior of bolts and the influence of the bolt diameter on the bearing strength of GFRPs were studied experimentally and numerically [18–24]. FRP beam-column joint connection methods and their performance were also studied [25,26]. Lehman et al. investigated the energy dissipation of four different kinds of bracing joints. Experimental results showed that the four kinds of bracing joints could prevent beam damage better than welded joints [27].

Related works were also conducted by other researchers. Kapti et al. investigated the effects of preload moment on the bearing strength and failure mode in pin-jointed and bolted carbon–epoxy plates subjected to a traction force [28]. Davalos et al. used different types of I-section, and box-section members in the three-point and four-point bending tests to examine the mechanics of laminated beams and used a finite element analysis model to predict the deformation and strain of the FRP components [29]. Masarira performed a finite element modeling of portal frames and established that a consistent relationship exists between the critical load for lateral-torsional buckling of the frame beams and the joint design [30]. Hejll et al. used a large size mixed ratio of GFRP composite beams in the four-point bending test and conducted a finite element analysis to compare the shear effect with that of the four-point bending test [31].

Other researchers focused on the numerical analysis of the frame, such as Li et al., who proposed the “equivalent column model” concept to analyze the brick panel inside RC frames. The numerical-analysis results could reasonably predict the lateral force-displacement relationships of these RC frames [32]. Gray and McCarthy developed a global bolted joint model (GBJM) for bolted composite joints. The GBJM was validated using both three-dimensional finite element models and experiments on both single-and multi-bolt joints [33]. Balc et al. conducted a finite element analysis of a beam to column end plate bolted connection using ABAQUS finite-element software (ABAQUS Inc., Johnston, RI, USA). The model was simplified by the use of finer mesh in areas of potentially high stress, namely the support regions and the contact areas [34].

This paper focuses on the mechanical behavior of glass fiber reinforced plastics (GFRP) frames made by assembling GFRP components with steel joints and bolts. A total of six GFRP frames, including single-span and double-span frames with and without diagonal bracing members, were tested using the pushover test to obtain the lateral load-displacement relationships of the GFRP frames. The linear stiffness, maximum load, dissipated energy, and failure modes of the GFRP frames were investigated. Numerical analysis was also performed to obtain the lateral load-displacement relationships of the GFRP frames. The analysis results were compared with the experimental results to show that the numerical-analysis results could reasonably predict the experimental force-displacement relationships of the GFRP frames.

2. GFRP Frame and Experimental Setup

2.1. GFRP Frame

The GFRP frames were made by double-web I-sections of the beam and column GFRP members with steel joints. The diagonal bracing is a rectangular section of the GFRP tube member. The schematic single-span and double-span GFRP frame configurations with dimensions are shown in Figures 1 and 2, respectively. In those figures, “F” denotes a frame form; the second letter “P” denotes that beam and column components are assembled by using steel joints and bolts. The number “1” denotes that the frame is a single-span frame, and the number “2” denotes that the frame is a double-span frame. Then, the next letter “T” denotes that the frame has a tension diagonal bracing, while the letter “C” denotes that the frame has a compression diagonal bracing. For example, the Frame FP2TC is a double-span frame with steel joints and bolts and has a tension diagonal bracing in the first (left) frame and a compression diagonal bracing in the second (right) frame as shown in Figure 2.

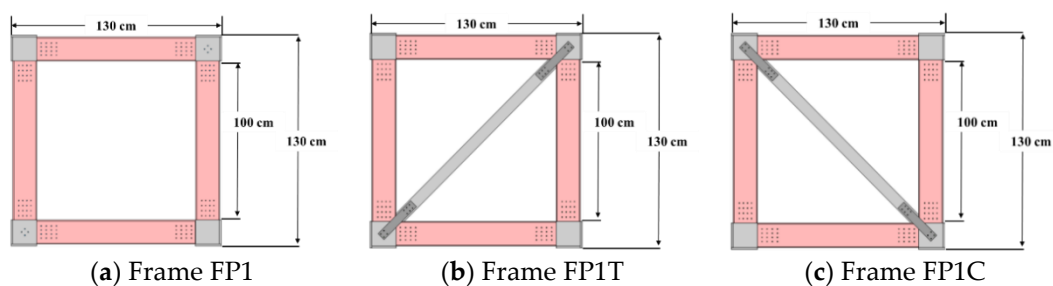


Figure 1. Schematic configuration of single-span GFRP frames.

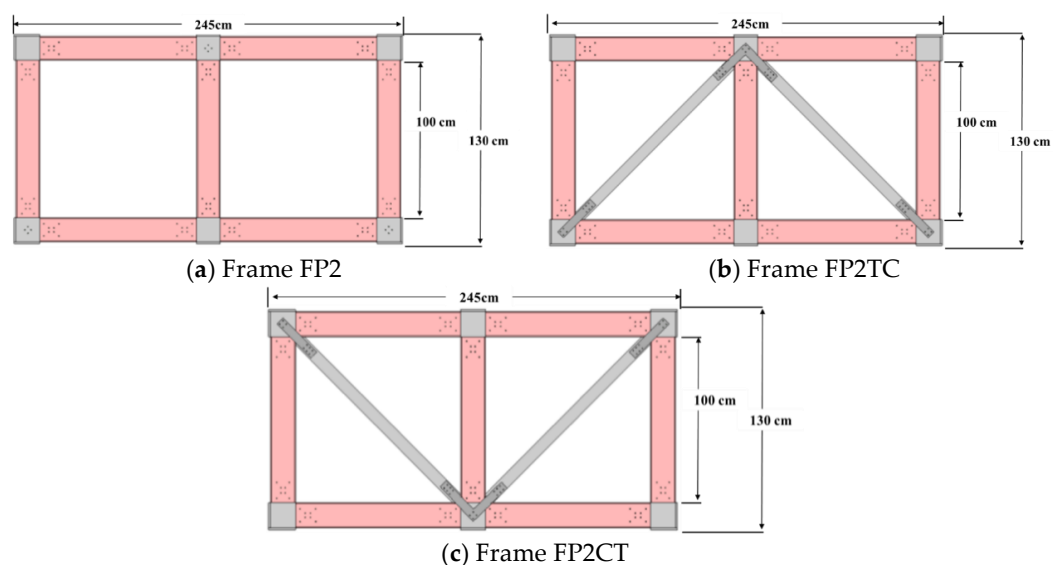


Figure 2. Schematic configuration of double-span GFRP frames.

Both the height and length of the single-span GFRP frame are 130 cm, and the height and length of the double-span GFRP frame are 130 cm and 245 cm, respectively. The dimension of the steel joint is 15 cm deep and 3.3 cm in thickness, shown in Table 1. The M6-4.8 bolt, whose diameter is 6 mm and shear strength is 192 MPa, was used to connect the GFRP members with the steel joints. The GFRP diagonal bracing is attached to the steel joint by using a steel block, and the steel block was inserted inside the GFRP bracing to avoid damage to the GFRP bracing from shearing. The above material and members used in the GFRP frame are shown in Table 1, and the sections and material properties of the GFRP members are shown in Table 2. The Elastic modulus was obtained from the three-point bending test [14,17].

Table 1. The material's member used in the GFRP frame.

| Member | Section | Specification |
|--------------------------------------|---------|--|
| GFRP double web I type component | | As beams and columns of the GFRP frame |
| GFRP rectangular tube type component | | As bracings of the GFRP frame |
| Metal joint | | As the beam-column joint |
| Bracing joint | | For locking the bracings to the frame joint |
| Filling steel block | | Inserted inside the GFRP bracing to avoid damage of the bracing from shearing due to bolt pressure |

Table 2. The sections and material properties of the GFRP members.

| Material Property | Section | |
|---------------------------------------|--------------|--------------|
| | | |
| Area (cm ²) | 23.47 | 5.23 |
| Moment of inertia (cm ⁴) | 848.56 | 35 |
| Elastic modulus (kN/cm ²) | $E_x = 1722$ | $E_x = 1722$ |
| | $E_y = 551$ | $E_y = 551$ |
| | $E_z = 551$ | $E_z = 551$ |

Note: x-direction is the fiber direction.

2.2. Experimental Setup

The GFRP frames are classified as single-span and double-span frames, and the setup of the pushover test for double-span frames is as shown in Figure 3. Each setup is composed of a reaction force frame, on which the hydraulic jack is mounted, and a fixation frame for the GFRP frame to rest on. The reaction force steel frame is fitted with a steel bedplate, and the GFRP frame is fitted with bolts to this steel bedplate.

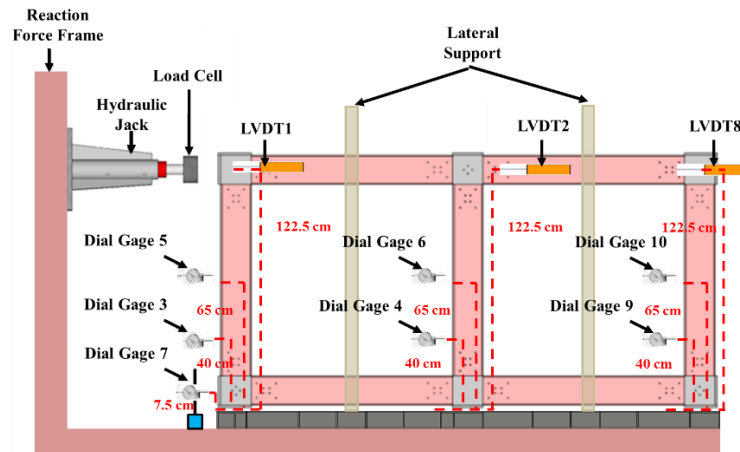


Figure 3. The experimental setup configuration of the double-span GFRP frame.

A displacement controlled pushover test was conducted with unidirectional loading. In order to avoid external deformation of the GFRP frame, two lateral supports were provided along with pulley rollers attached to them to reduce the in-plane deformation from friction. Data from the Load Cell, Linear Variable Differential Transformer (LVDT) sensors, and Dial Gages are synchronized to measure forces and displacements.

The hydraulic jack can apply a maximum force of 10 metric tons load and a stroke of 27 cm; the load cell (WF 17120, Wykeham Farrance, Milan, Italy) with 50 tons capacity was utilized to measure the load imposed by the hydraulic jack, dial gage (DDP-30A, Tokyo Sokki Kenkyujo Co., Ltd., Tokyo, Japan), and LVDT (SDP-100C, Tokyo Measuring Instruments Lab., Tokyo, Japan) was utilized to measure the displacements. A high precision data logger (KL-10, Geomaster Group, Tianjin, China) was used to record the force and displacement data, and a sampling rate of 1 data/sec was set to record the force-displacement information.

In Figure 3, three displacement sensors (LVDT1, LVDT2, and LVDT8) are placed on the columns at a distance of 122.5 cm from the bottom of the frame. The dial gages DG5, DG6, and DG10, are situated 65 cm from the bottom of the frame on the columns. Other dial gages are mounted 40 cm from the bottom of the frame, DG3, DG4, and DG9. A dial gage is also positioned 7.5 cm from the bottom of the left column (DG7) to measure any slip or slide on the bedplate. Drift ratio measurements are similar to the method used for the single-span frames.

3. Experimental Observations and Discussions of the Pushover Test

The observations during the pushover tests of the GFRP frames are presented below, as well as the force-displacement relationship and the energy dissipation of the GFRP frames.

3.1. Single-Span Frames

Three groups of single-span GFRP frames in the form of the force-displacement relationship diagram, and their failure modes are presented below. And the energy dissipations are compared for the three single-span GFRP frames.

3.1.1. Frame FP1

The setup of the pushover test for Frame FP1 is shown in Figure 4. The measured force-displacement relationship curve of Frame FP1 during the pushover test is shown in Figure 5. As the drift ratio reached 1.5% and the force reached 20 kN, there was a subtle splitting sound. As the drift ratio reached 3.0% and the force reached 31 kN, cracking commenced around the bolts in the lower-left corner of the GFRP column where the steel joint is connected. As the drift ratio reached 4.0% and the force reached 33 kN (with a displacement of 5 cm), the upper-left corner column member also cracked around the bolts in the joint. As the drift ratio reached 4.5%, the lower-right corner column member exhibited the same cracking around the joint. As the drift ratio reached 5.0%, the upper-right corner of the upper beam member cracked at the joint location around the bolts. As the drift ratio reached 6.0%, the loading was stopped, and the maximum displacement at this time was 7.4 cm. The Frame FP1T has a tension bracing, and the failure mode is tearing of tension bracing. Frame FP1C has a compression bracing, and the failure mode is the buckling of the compression bracing. As shown in Figure 5, the stiffness of the Frame FP1T and Frame FP1C are different; the reason might be that the ultimate tensile strength of the GFRP member is greater than that of the compressive strength and their failure modes are different. The detailed damage photos of Frame FP1 are shown in Figure 6.

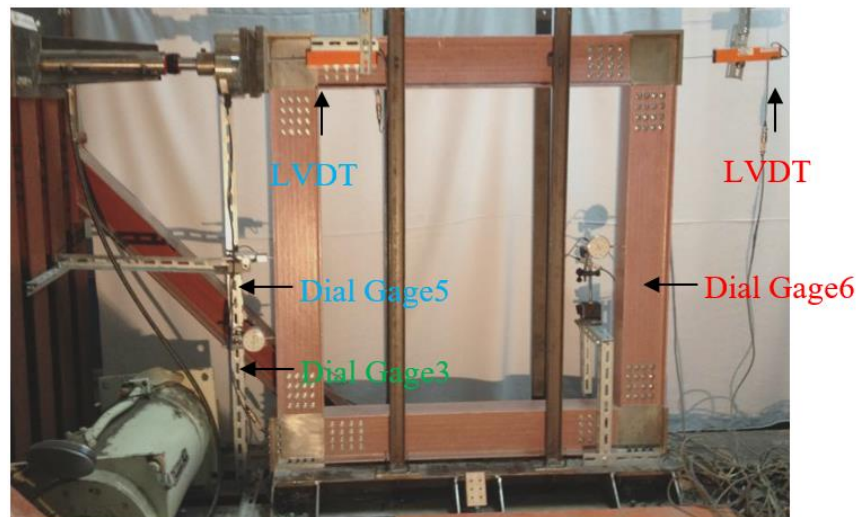


Figure 4. The experimental setup of Frame FP1.

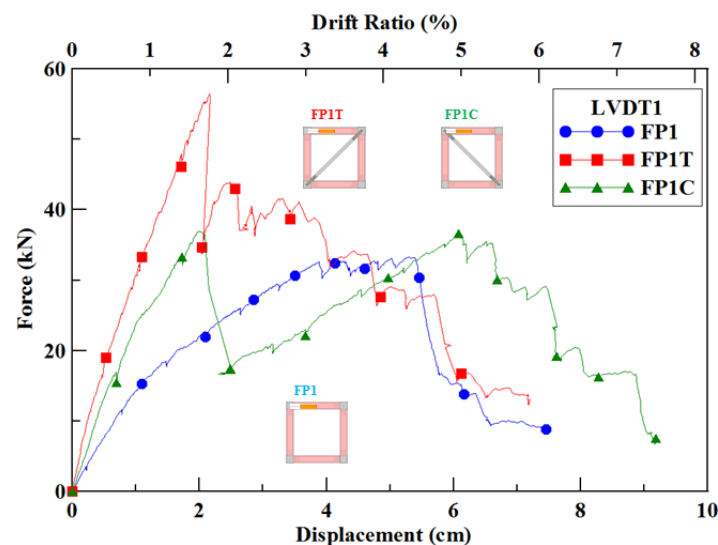


Figure 5. The experimental force-displacement relationship of single-span GFRP frames.

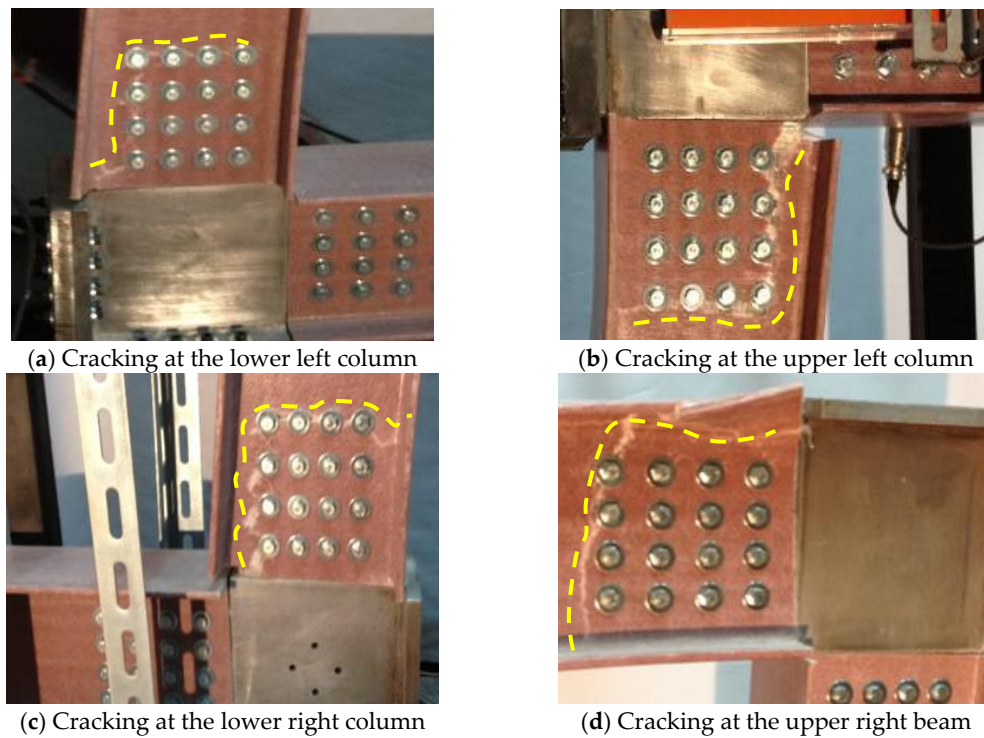


Figure 6. The damaged photos and locations of the Frame FP1.

3.1.2. Frame FP1T

The measured force-displacement relationship curve of Frame FP1T during the pushover test, as previously shown in Figure 5. When the LVDT1 measured a drift ratio of 2.0%, the tensile diagonal bracing was torn at the upper-right corner joint, causing the failure of the diagonal bracing member. The force at this time was about 56 kN, and the displacement was about 2.2 cm. After the failure of the brace, the force dropped to 35 kN. After this point, any further loading was directly sustained by the frame itself. When the LVDT1 measured a drift ratio of 3.0%, the lower-left column member cracked at the joint area around the bolts. The load at this time was about 40 kN, and the displacement was 3.6 cm. When the LVDT1 measured a drift ratio of 5.0%, the upper-right corner column member experienced tearing at the joint around the bolts, then the lower-right corner column member also suffered the same failure. When the LVDT1 measured a drift ratio of 6.0%, the loading was stopped, and the maximum displacement was 7.2 cm. The damage photos of tension diagonal bracing of Frame FP1T are shown in Figure 7.

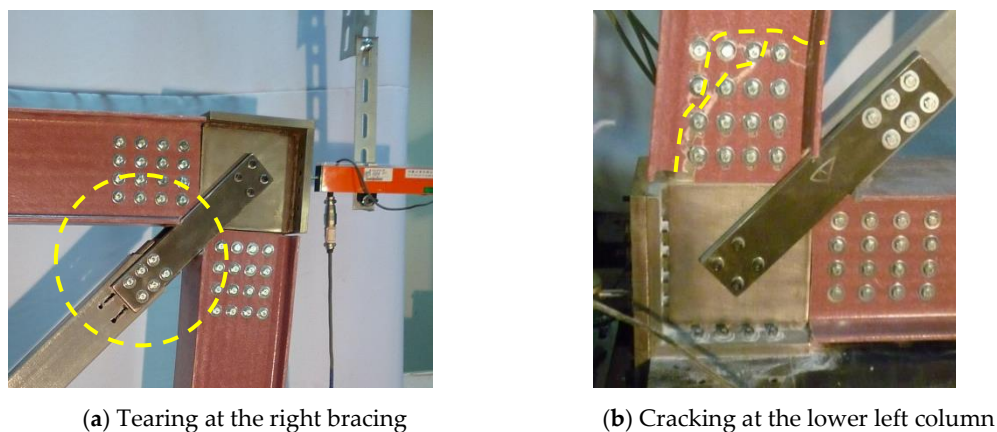


Figure 7. The damage photos of the tension diagonal bracing of Frame FP1T.

3.1.3. Frame FP1C

The force-displacement relationship curve of Frame FP1C is previously shown in Figure 5. When the LVDT1 measured a drift ratio of 2.0%, the compression diagonal bracing buckled. At this time, the force was 37 kN, and the displacement was 2.0 cm. After the diagonal bracing failed, the load dropped to 17 kN, and from this point, any further loading was directly sustained by the frame itself. When the LVDT1 measured a drift ratio of 5.0%, the lower-left corner of the column member began to crack at the joint around the bolts. At this time, the force was about 36 kN, and displacement was about 6.0 cm. When the LVDT1 measured a drift ratio of 6.0%, the upper-left corner column member exhibited the same cracking. When the LVDT1 measured a drift ratio of 6.5%, the lower-right corner column member followed the same pattern. When the LVDT1 measured a drift ratio of 7.0%, the loading was stopped, and the maximum displacement was 8.6 cm. The damage photos of Frame FP1C are shown in Figure 8.

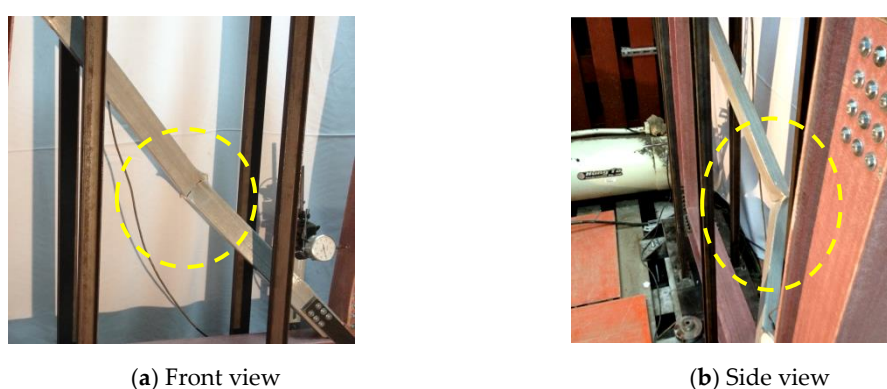


Figure 8. The damage photos of the diagonal bracing of Frame FP1C.

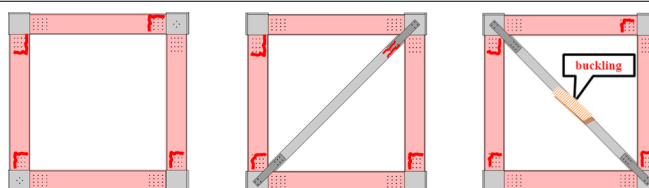
3.1.4. Comparison of the Three Single-Span Frames

The experimental results of the three single-span GFRP frames are shown in Table 3. The force-displacement relationship curves of the three single-span frames are previously shown in Figure 5. Frame FP1T and Frame FP1C have better stiffness and ultimate strength at the initial stages than the prototype Frame FP1. This proves that adding a brace can improve the overall stiffness and strength of the frame. GFRP has higher tensile than compressive strength; therefore, the ultimate strength of Frame FP1T is even higher than that of Frame FP1C.

Table 3. The experimental results of the three single-span GFRP frames.

| Frame | FP1 | FP1T | FP1C |
|---|-------|-------|-------|
| Linear Stiffness (kN/cm) | 15.9 | 42.2 | 26.2 |
| Ultimate Strength (kN) | 33.3 | 56.4 | 36.9 |
| Relative Displacement at Ultimate Strength (cm) | 4.8 | 2.0 | 1.4 |
| Drift Ratio (%) | 3.9% | 1.6 | 1.1 |
| Dissipated Energy * (kN-m) | 154.5 | 216.9 | 192.3 |

Failure Locations



* Dissipated energy was calculated with drift ratios of up to 6%.

If the GFRP frames contain diagonal bracing, the bracing members become the first casualty, whether in tension (tearing) or in compression (buckling) damage. Diagonal bracing damaged by tension occurs in the form of bolt hole tearing by the bolts due to a high concentration of stress. Diagonal bracing damaged by compression is visible when the bracing member buckles. This buckling phenomenon serves as an early warning and may present an opportunity for the compression diagonal bracing to be repaired/replaced/reinforced before failure. After the destruction of the diagonal bracing member, the frame itself starts to fail with continuous loading. The bottom left corner of the GFRP column cracks along with the bolts. Then, the upper left corner column member fails, cracking along the bolt openings. After this, the bottom right corner column member fails by cracking along the bolt openings. The energy dissipation relationship diagram of the three single-span GFRP frames are shown in Figure 9. As seen from Figure 9, the dissipation energy of Frame FP1T is the highest, followed by Frame FP1C and finally Frame FP1. Since the tensile strength of GFRP composite material is greater than that of compressive strength. The Frame FP1T has a tension bracing, and Frame FP1C has a compression bracing. Therefore, the initial stiffness of FP1T is better than that of FP1C under the pushover test.

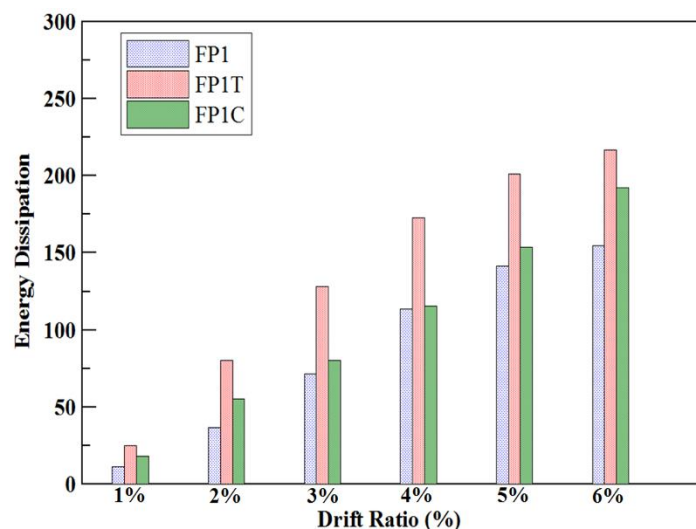


Figure 9. The energy dissipation-drift ratio relationships of single-span frames.

3.2. Double-Span Frames

This section presents the force-displacement relationship curves and their corresponding failure modes of three double-span GFRP frames. And the energy dissipations are compared for the three types of GFRP frames.

3.2.1. Frame FP2

The schematic of the Frame FP2 experimental setup is shown in Figure 10. The force-displacement relationship curve of Frame FP2 is shown in Figure 11. When the LVDT1 measured a drift ratio of 4.5%, a loud splitting sound was heard, and the force at that time was recorded as 42 kN with the displacement equal to 5.4 cm. The lower part of the left column began to deform in the joint area distorting the bolt openings. Next, the upper left joint, middle-upper joint, middle-lower joint, and the bottom-right joints began to deform from the relative rotation of the GFRP members against the steel joints.

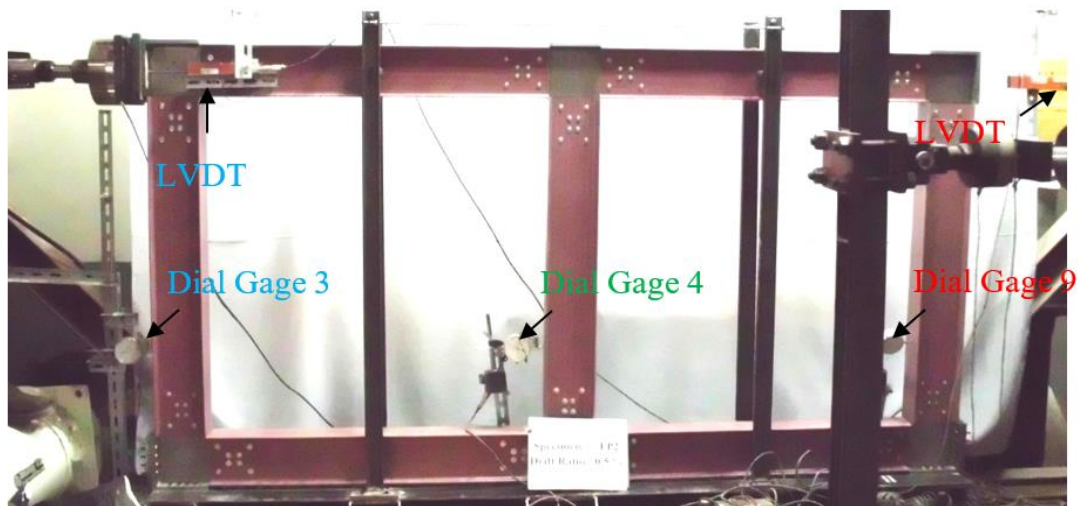


Figure 10. The experimental setup of Frame FP2.

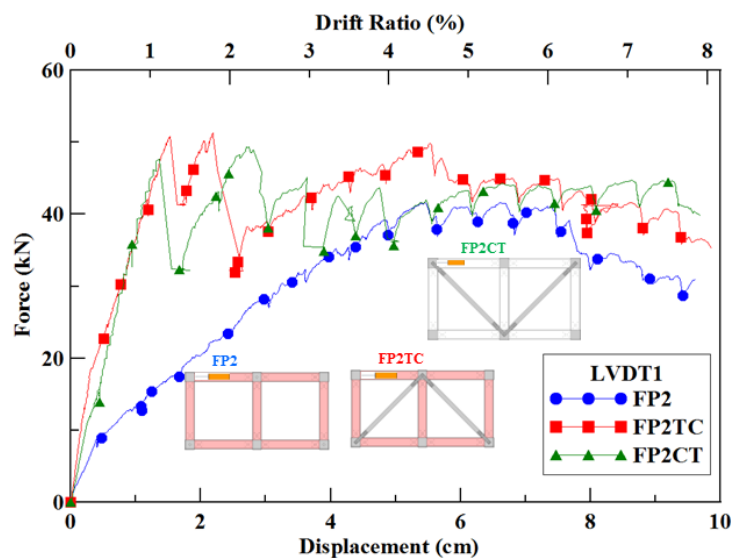


Figure 11. The experimental force-displacement relationships of the double-span GFRP frame.

When the LVDT1 measured a drift ratio of 6.0%, a second splitting sound was heard, and the force was recorded as 40 kN with the displacement equal to 7.4 cm. The lower part of the left column exhibited cracking around the bolt openings, and the force dropped after this failure. The upper corner of the left column bulged at the flange from the impact of the steel joint. The upper and lower parts of the middle column also bulged from impact with the steel joints. The upper right corner of the beam slightly bulged at the flange near the steel joint, and the same thing happened at the lower right corner of the right column. When the LVDT1 measured a drift ratio of 8.0%, the loading was stopped at the maximum displacement of 9.6 cm. The detailed damage photos of Frame FP2 are shown in Figure 12.

3.2.2. Frame FP2TC

The force-displacement relationship curve of Frame FP2TC is previously shown in Figure 11. When the LVDT1 measured an approximate drift ratio of 1.5%, the compression bracing (right) failed in buckling at a force of about 51 kN and a displacement of 1.7 cm. When the LVDT1 measured a drift ratio of 2.0%, the lower-left corner of the tension diagonal bracing joint tore along the bolt openings. At this time, the force was about 51 kN with a displacement of 2.4 cm. The upper corner of the left column bulged at the flange from impact with the steel joint. The upper and lower ends of the middle

column also showed signs of impact by the steel joint. The upper right corner of the beam and the right column underwent rotation but showed no significant damage. The lower corner of the right column flange was also slightly impacted by the steel joint. Then LVDT1 measured a drift ratio of 8.0%, then the force was stopped at the maximum displacement of 9.6 cm. Frame FP2TC's comprehensive damage images are shown in Figure 13.

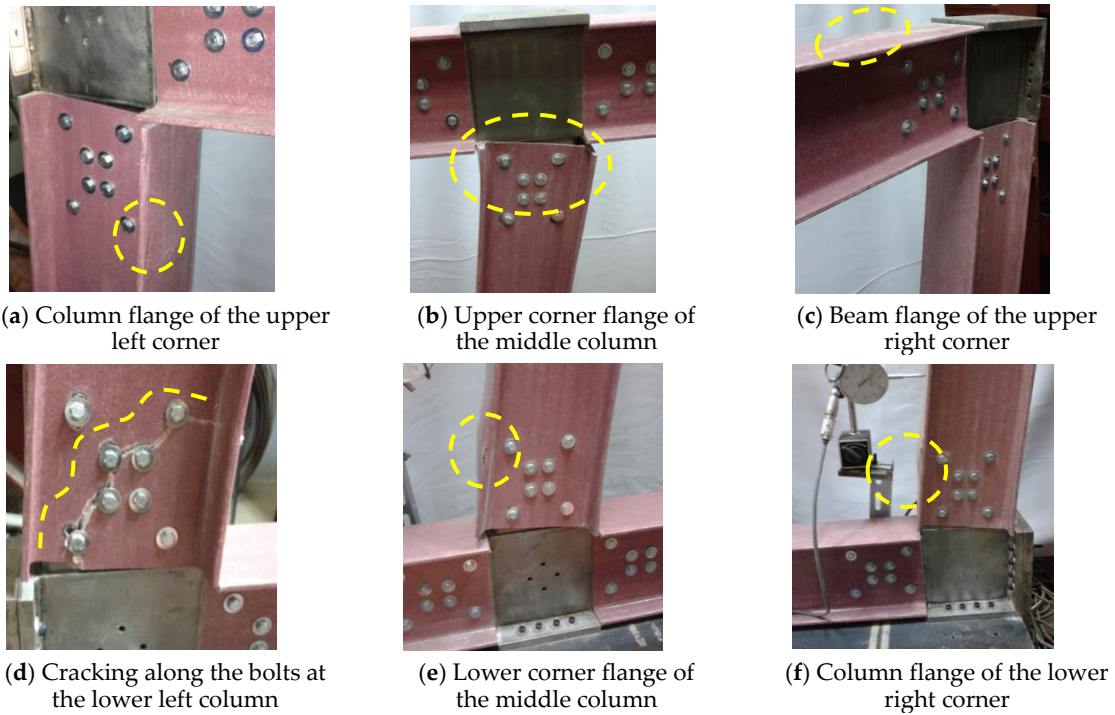


Figure 12. The damage photos and locations of Frame FP2.

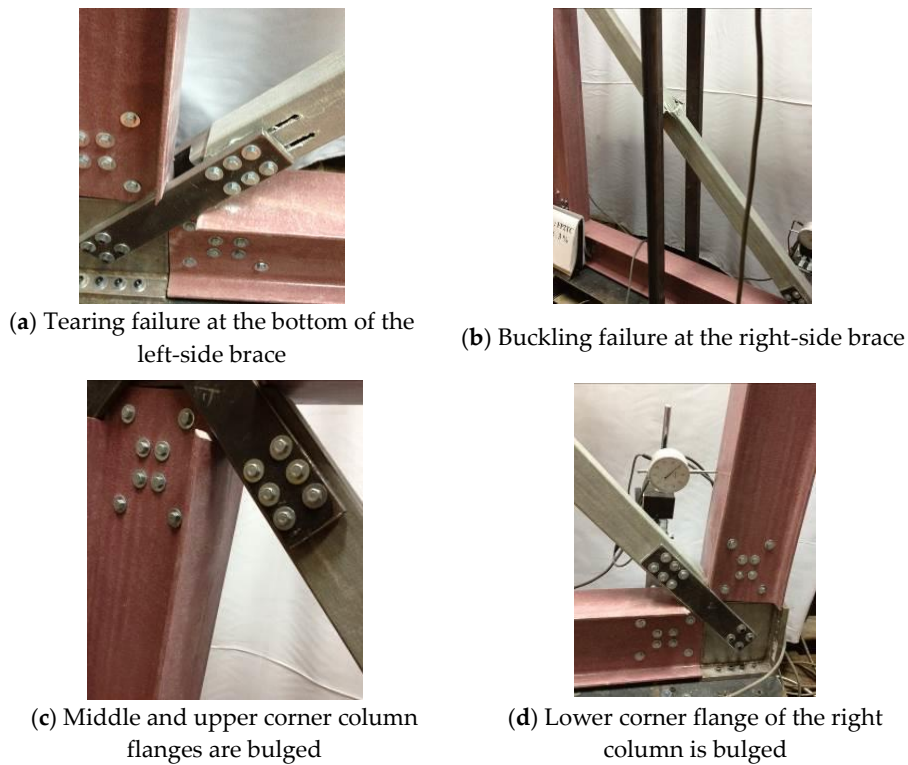


Figure 13. The damage photos and locations of Frame FP2TC.

3.2.3. Frame FP2CT

Previously, the Frame FP2CT force-displacement relationship curve is shown in Figure 11. The LVDT8 encountered measuring errors, so its recorded data was not used. When the LVDT1 measured a drift ratio of 1%, the left brace buckled in compression damage. At this time, the force was about 48 kN and the displacement was nearly 1.4 cm. Then LVDT1 measured a drift ratio of 2.0%, the lower-left corner joint on the right side cracked with a force of about 49 kN, and a displacement of 2.7 cm. The flange on the left end of the upper beam was cracked from the bracing kit, moving against it. In the middle column, both ends were distorted and cracked at the edge of the web from contact with the steel joints. There was a slight rotation in the upper right corner of the frame when the beam meets the column. The flange at the lower end of the right column was also slightly impacted by the steel joint. As the LVDT1 measured a drift ratio of 8.0%, loading was stopped at the maximum displacement of 9.7 cm. The detailed damage photos of Frame FP2CT are shown in Figure 14.

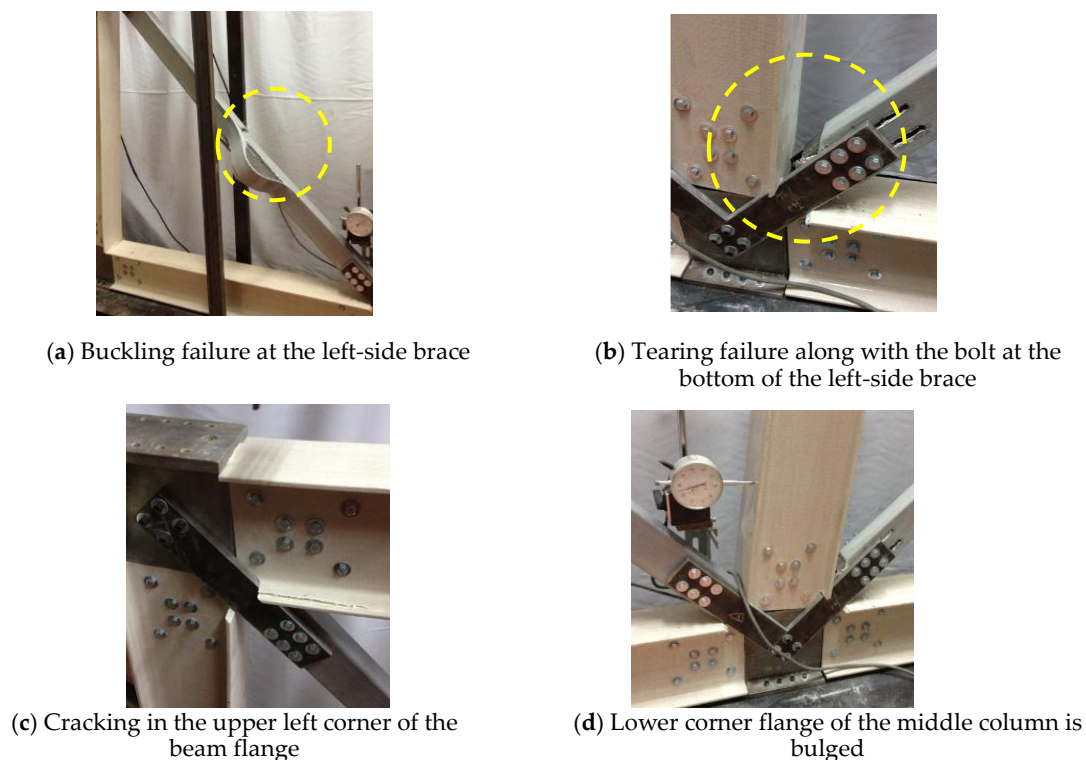


Figure 14. The damage photos and locations of Frame FP2CT.

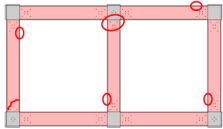
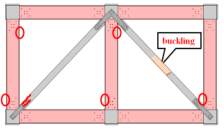
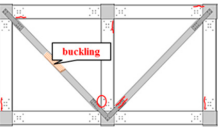
As seen from Figures 12–14 of the damage photos of the double-span GFRP frames, we can conclude that the compression bracings were buckled failure, the tension bracings were tearing failure, and the columns were cracking along the bolts.

3.2.4. Comparison of the Three Double-Span Frames

The experimental results of the three double-span GFRP frames are shown in Table 4. The force-displacement relationship curves of the three double-span frames are previously shown in Figure 11. Frame FP2TC and Frame FP2CT have better stiffness and ultimate strength than the prototype Frame FP2 at the initial stages. This proves that adding bracing can improve the overall strength and stiffness of the frame. Additionally, the first failure mode is the buckling of the compression bracing followed by tearing of the extension bracing along the bolt openings. The compression bracing buckling can serve as an early warning, and the bracing member can be replaced immediately to prevent further damage to the frame.

Table 4. The experimental results of the double-span GFRP frames.

| Frame | FP2 | FP2TC | FP2CT |
|--|-------|-------|-------|
| Linear stiffness (kN/cm) | 20.8 | 60.1 | 43.8 |
| Maximum load (kN) | 41.6 | 51.3 | 49.4 |
| Relative displacement at maximum load (cm) | 5.4 | 2.2 | 2.7 |
| Drift ratio (%) | 4.5 | 1.8 | 2.2 |
| Dissipated energy * (kN-m) | 212.4 | 300.9 | 282.6 |

* Dissipated energy was calculated when the drift ratio is up to 6%.

After the bracing fails, the next point of failure is the lower end of the left column, which cracks along the bolts. The upper left corner of the frame bulges and cracks along the beam flange due to contact with the bracing kit. Then, the middle column bulges at both the upper and lower end from contact with the steel joints. The upper corner of the frame rotates, and the beam edge exhibits cracking. The lower right corner column flange is impacted by the steel joint.

The energy dissipation relationship diagram of the three double-span frames is shown in Figure 15. Energy dissipation is best in the Frame FP2TC, followed by Frame FP2CT and finally by Frame FP2.

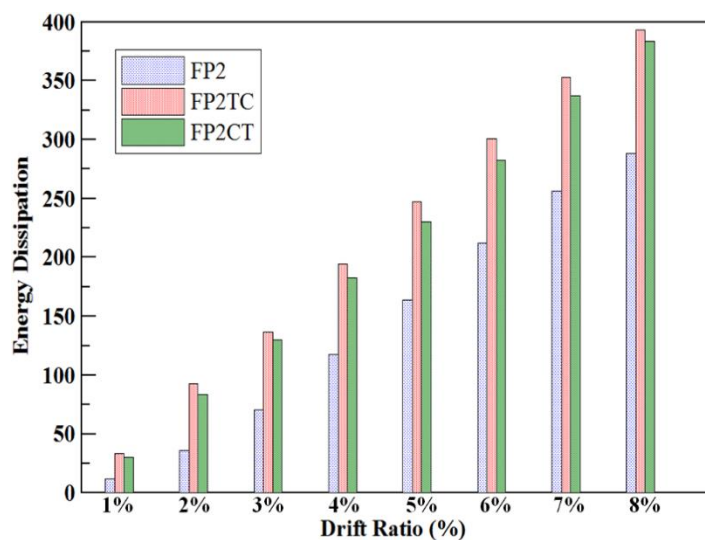


Figure 15. The energy dissipation-drift ratio relationships of the double-span frames.

4. Nonlinear Pushover Numerical Analysis

In nonlinear pushover analysis, 2D models of the frames were numerically analyzed using SAP2000 Version 14 [35]. The model created with the dimensions and material properties of the experimental GFRP frames were analyzed by the software. The left and right lower ends of the frame are assigned fixed supports at the steel joints (also the middle-lower joint in the case of double-span frames). The material parameters of the GFRP components are given in Table 2. Plastic hinges were manually defined for each column member, one in the upper part and one in the lower end. A plastic hinge was also defined in the middle of each bracing member.

The nonlinear nature of the problem requires the use of plastic hinges to simulate the behavior of the frame after yielding. Before yielding, the frame is in an elastic state, and the elastic behavior takes place over the entire length of the member. However, once the yielding point is reached, deformation behavior will be propagated from the hinges. Plasticity may be defined by the force-displacement

relationship or moment-rotation relationship. The SAP2000 software; however, limits the negative slope to 10% of the elastic stiffness, so the hinge-overwrite option was used to simulate the force decrease after failure.

The plastic hinge parameters were set by using a single-column force-displacement relationship diagram and converting it into a moment-rotation relationship. Then the moment-rotation relationship was normalized and applied in the software to set the plastic hinge locations. We subtracted the force-displacement relationship of the prototype frame from that of the braced frame to obtain the force-displacement relation of the brace itself [30]. Then, the force-displacement relationship of the bracing was normalized and applied in the software to set the plastic hinge. The span of the frame was set in the x-axis, and the frame height in the z-axis. Using the parameters obtained from the above procedures, “Hinge-overwrites” was set using the built-in commands of SAP2000. When one or more plastic hinges were set, the Hinge-overwrite parameter could be used with location setting between 0 and 1. The illustration figure of the structural analysis model and the locations of the plastic hinge of Frame FP2CT is shown in Figure 16.

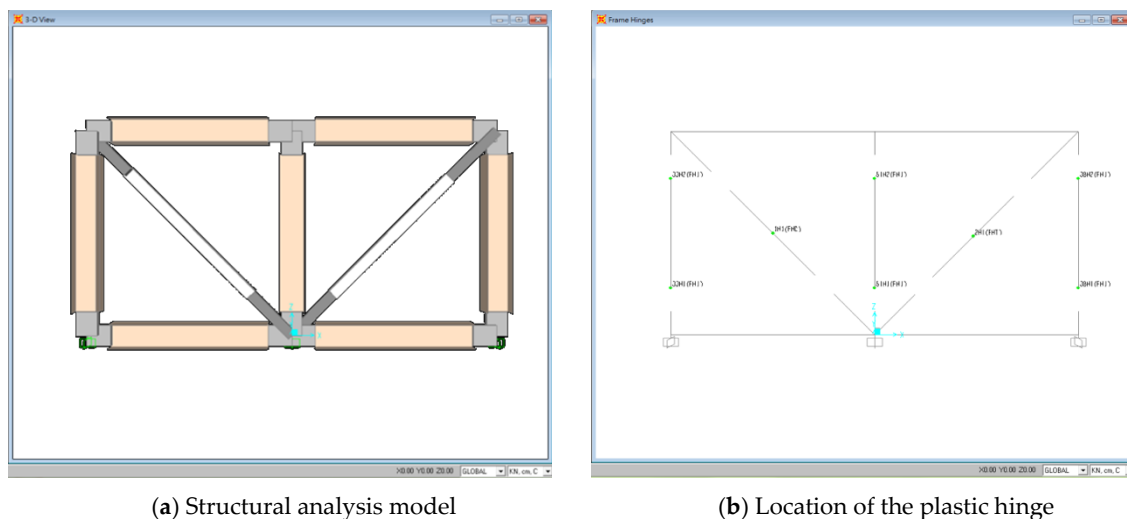


Figure 16. The illustration figure of the structural analysis model and the locations of the plastic hinges of Frame FP2CT.

In the case of Frame FP1 shown in Figure 17, the dotted curve in blue represents the experimental results, and all the other curves were obtained by trial and error of the plastic hinge locations. The parameters were first set without the hinge-overwrite parameter, but the analysis could not simulate the curve at failure. When the plastic hinges were set at 0.9, the strength started to drop after a drift ratio of almost 4%. The hinge locations were varied, and when the value reached 0.2, the numerical-analysis curve (solid triangles in red) had a trend similar to the experimental results. When the parameter was set to 0.1, the analysis showed an unstable curve. Therefore, the hinge-overwrite parameter in Frame FP1 was set using a plastic hinge of 0.2.

The hinge-overwrite settings allow for proper simulation of plastic hinge locations. The plastic hinge allows the transfer of moment, and as such, the analytical behavior of the model can be made to simulate the behavior of the experimental GFRP frames. The hinge overwrites option in this manuscript was adjusted according to the experimental results. Table 5 gives the recommended hinge-overwrite coefficients to fit the experimental force-displacement curve. For single-span and double-span GFRP frames, the hinge-overwrite coefficients of the column were set as 0.2 and 0.6, respectively. For single-span frames, the hinge-overwrite coefficients of both tension and compression bracings were set as 0.09. For double-span frames, the hinge-overwrite coefficients of tension bracings of FP2TC and FP2CT were set as 0.2 and 0.4, respectively; the compression bracings were set as 0.1. Through more experimental data, we can learn from the big data and conclude the proper values of the

hinge-overwrite coefficients for different GFRP structural members. The numerical structural analysis of the GFRP frame depends on the data of the moment versus rotation relationship derived from the experiment and the hinge-overwrite coefficients. The performed structural analysis in this manuscript may not be feasible for different GFRP structural members and systems.

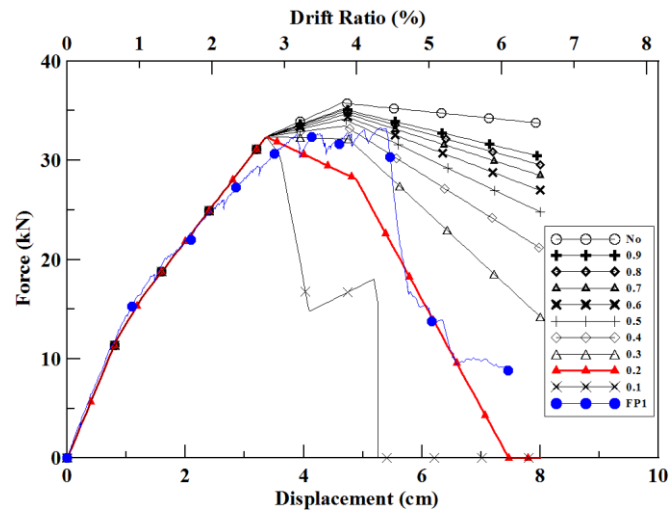


Figure 17. The force-displacement relationships of Frame FP1 using different hinge-overwrite parameters.

Table 5. The hinge-overwrite coefficients used in the numerical analysis.

| Frame | Column | Tension Bracing | Compression Bracing |
|-------|--------|-----------------|---------------------|
| FP1 | 0.2 | - | - |
| FP1T | 0.2 | 0.09 | - |
| FP1C | 0.2 | - | 0.09 |
| FP2 | 0.6 | - | - |
| FP2TC | 0.6 | 0.2 | 0.1 |
| FP2CT | 0.6 | 0.4 | 0.1 |

5. The Comparison of the Experimental and Numerical Analysis Results

The force-displacement relationships of the experiments and numerical analysis of GFRP frames were compared, and the findings are discussed below. The detailed comparison results of the six GFRP frames are discussed as follows.

The frame FP1 drift ratio moves from 0 to 3%; the experimental and numerical-analysis curves follow a close trend, as shown in Figure 18a. The analysis curve's initial stiffness is similar, but the force is started to decrease after a drift ratio of 3%, while that of the experimental curve decreased after a drift ratio of 4%. The overall trend lines are similar.

The experimental and numerical-analysis trend lines of Frame FP1T are very close at the drift ratio is between 0 and 1.8 %, and the initial stiffness lines are also similar. After a drift ratio of 1.8%, the force in the analysis curve began to decline. The analysis simulated the experiments bracing tension failure. Therefore, the prototype frame was able to sustain the loading after the force decreased so that the force rose again. The numerical-analysis and experimental curves for Frame FP1T are similar, as shown in Figure 18b.

From the drift ratio of 0 to 1.8%, the experimental and numerical-analysis trend lines of Frame FP1C are very close, as shown in Figure 18c; the bracing buckles and the force decrease after a drift ratio of 1.8%. Comparing the analysis of Frame FP1C with the prototype Frame FP1, it shows that the force decreases in Frame FP1C at the drift ratio of 1.8%, and the loading force is close to that of

Frame FP1. This shows that the frame itself is now sustaining the loading directly as Frame FP1 is not braced. However, in the experiment, the force decreased after the drift ratio was greater than 1.8%, which could be attributed to the failure of the load cell to catch up with the frame after the bracing buckled. The recovery numerical-analysis trend of the Frame FP1C, after the bracing buckled, is similar to the experimental curve of Frame FP1.

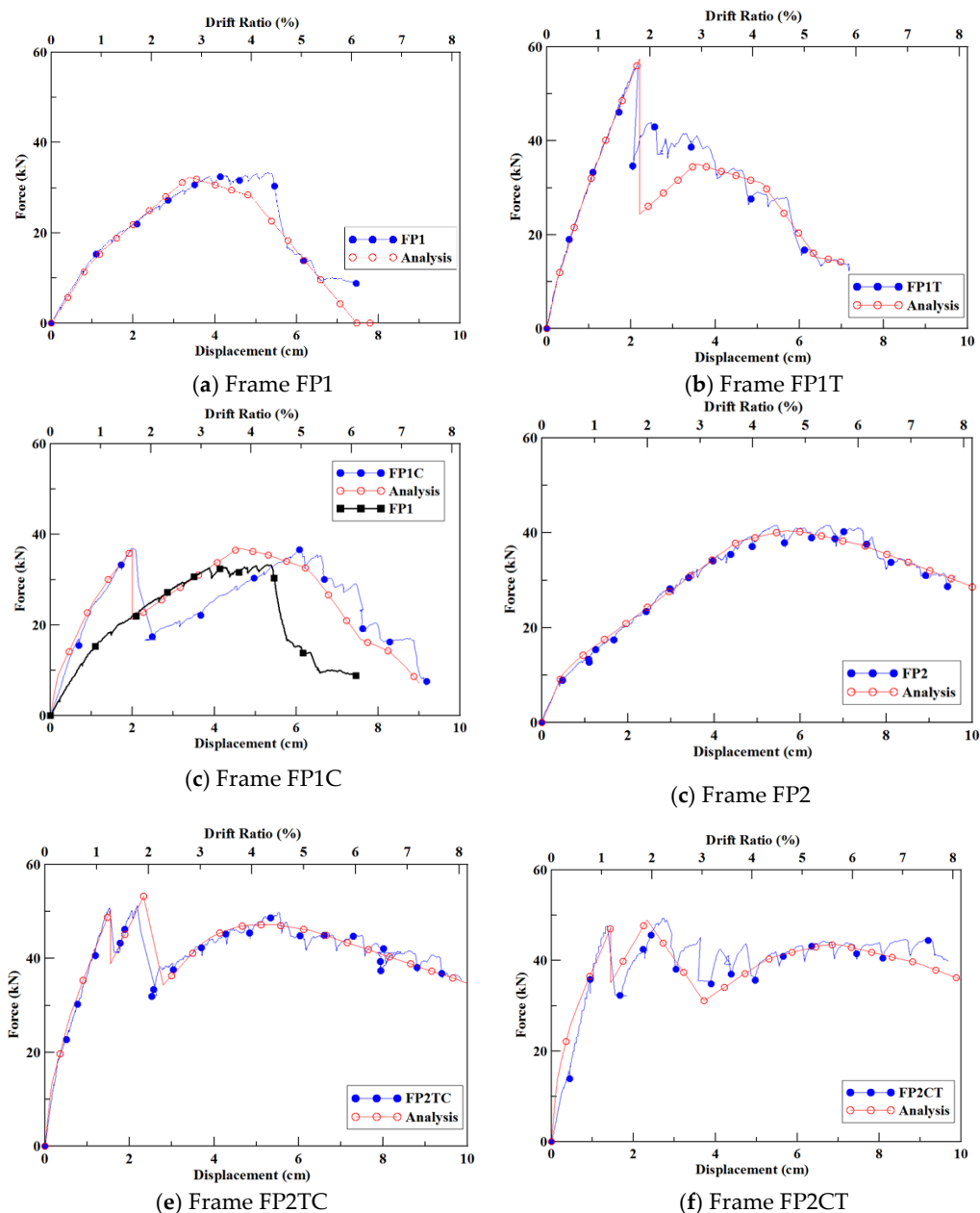


Figure 18. The experimental and numerical-analysis force-displacement relationships of all the GFRP frames.

The experimental and numerical-analysis trend lines of Frame FP2 as shown in Figure 18d. Both trend lines are similar at a drift ratio between 0 and 6%, and the initial stiffness lines are similar, as well. After a drift ratio of 6%, the experimental curve shows a lower force than the analysis curve. Overall, the comparison is very good.

The experimental and numerical-analysis trend lines of Frame FP2TC are very close as shown in Figure 18e, and the initial stiffness lines are also very similar, which means that the analysis can be used to simulate the experiment effectively. The first failure occurs at the drift ratio of 1.2% when the

compression bracing buckles and the force drops. The force increases back up to a drift ratio of 1.8% when the tension bracing also fails, and the force drops again. Finally, the frame takes up the loading, and the force increases slightly. The relationships between the experimental and numerical-analysis force-displacement are identical and follow the same trend with little differences.

The experimental and numerical-analysis trend curves of Frame FP2CT are shown in Figure 18f. The experimental observation shows that the compression bracing's first failure occurs at a drift ratio of 1%, causing a drop in force. After the force increases up to a drift ratio of 2%, when the tension bracing also fails. The force then drops again, and as the frame takes up the loading, it increases again. The experimental and numerical-analysis force-displacement relationships are identical and follow the same trend.

The error in the ultimate loads between the experimental and numerical-analysis results are shown in Table 6. The numerical-analysis results show that the error rate is less than 4% when compared with the experimental results. This numerical-analysis demonstrates that the use of SAP2000 simplifies the work of engineers because the analysis software has an acceptable accuracy and simulation capability.

Table 6. The errors of the ultimate loads between the experimental and numerical-analysis results.

| Frame | Ultimate Strength (kN) | | |
|-------|------------------------|--------------------|--------------------|
| | Experiment | Numerical Analysis | Absolute Error (%) |
| FP1 | 33.3 | 32.3 | 3 |
| FP1T | 56.4 | 57.4 | 1.8 |
| FP1C | 36.9 | 36.4 | 1.4 |
| FP2 | 41.6 | 40.4 | 2.9 |
| FP2TC | 51.3 | 53.2 | 3.7 |
| FP2CT | 49.4 | 48.9 | 1 |

6. Conclusions

From the experimental observations and the numerical-analysis results of this study, the following conclusions were drawn:

1. Single-span Frame FP1T with tension bracing had a 165% increase in initial stiffness and 69% increase in ultimate strength, and Frame FP1C with compression braced had a 65% increase in initial stiffness and 11% increase in maximum load.
2. Double-span Frame FP2TC had a 23% increase in initial stiffness and a 189% increase in ultimate strength, and Frame FP2CT had a 19% increase in initial stiffness and a 111% increase in ultimate strength. The failure mode of GFRP frames begins from the buckling of the compression brace. At this stage, there is no damage to the overall beams and columns, which means that the second component can be replaced as there is an early warning of failure.
3. Since the FRP composite material structural member is brittle, so the SAP2000 analysis was set up to analyze brittle material failure by using the hinge-overwrite command to simulate the GFRP frame's reaction to the pushover force.
4. The numerical structural results have an absolute error rate of less than 4% when they are compared with the experimental results. This proves the use of SAP2000 has an acceptable accuracy while saving time and cost in engineering practice.
5. The numerical structural analysis of the GFRP frame depends on the data of the moment versus rotation relationship derived from the experiment and the hinge-overwrite coefficients. The performed structural analysis in this manuscript may not be feasible for different GFRP structural members and systems.

Author Contributions: Conceptualization—Y.-F.L.; Methodology, —Y.-F.L.; Data Curation—J.-Y.L. and C.-C.Y.; Formal Analysis—J.-Y.L.; Writing-Original Draft Preparation—J.-Y.L. and C.-C.Y.; Writing-Review and Editing—Y.-F.L.; Supervision—Y.-F.L.; Project Administration—Y.-F.L.

Funding: This research was funded by the National Science Council of Taiwan under contract No. NSC-100-2622-E-027-027-CC3, and the “Research Center of Energy Conservation for New Generation of Residential, Commercial, and Industrial Sectors” from the Ministry of Education (MOE) in Taiwan.

Acknowledgments: The authors thank Walter Chen and Osman Jobe for their assistance with proofreading the manuscript. Also, the authors would like to thank the anonymous reviewers for their constructive comments that greatly improved the final version of this manuscript.

Conflicts of Interest: The authors declare no conflict of interest.

References

- Li, Y.F.; Yu, C.C.; Chen, S.Y.; Badjie, S. The carbon footprint calculation of the GFRP pedestrian bridge at Tai-Jiang National Park. *Intern. Rev. Spat. Plan. Sustain. Dev.* **2013**, *1*, 13–28. [[CrossRef](#)]
- Tang, Y.; Sun, Z.; Wu, G. Compressive Behavior of Sustainable Steel-FRP Composite Bars with Different Slenderness Ratios. *Sustainability* **2019**, *11*, 1118. [[CrossRef](#)]
- Karayannis, C.G.; Kosmidou, P.M.K.; Chalioris, C.E. Reinforced Concrete Beams with Carbon-Fiber-Reinforced Polymer Bars-Experimental Study. *Fibers* **2018**, *6*, 99. [[CrossRef](#)]
- Cevallos, O.A.; Olivito, R.; Codispoti, R. Experimental Analysis of Repaired Masonry Elements with Flax-FRCM and PBO-FRCM Composites Subjected to Axial Bending Loads. *Fibers* **2015**, *3*, 491–503. [[CrossRef](#)]
- Yazdanbakhsh, A.; Bank, L.C. A critical review of research on reuse of mechanically recycled FRP production and end-of-life waste for construction. *Polymers* **2014**, *6*, 1810–1826. [[CrossRef](#)]
- Correia, J.R.; Almeida, N.M.; Figueira, J.R. Recycling of FRP composites: Reusing fine GFRP waste in concrete mixtures. *J. Clean. Prod.* **2011**, *19*, 1745–1753. [[CrossRef](#)]
- Bakis, C.E.; Bank, L.C.; Brown, V.L.; Cosenza, E.; Davalos, J.F.; Lesko, J.J.; Machida, A.; Rizkalla, S.H.; Triantafillou, T.C. Fiber-reinforced polymer composites for construction—State-of-the-art review. *J. Compos. Constr.* **2002**, *6*, 73–87. [[CrossRef](#)]
- Kumar, P.; Chandrashekhara, K.; Nanni, A. Structural performance of a FRP bridge deck. *Constr. Build. Mater.* **2004**, *18*, 35–47. [[CrossRef](#)]
- Moon, D.Y.; Zi, G.; Lee, D.H.; Kim, B.M.; Hwang, Y.K. Fatigue behavior of the foam-filled GFRP bridge deck. *Compos. Part B* **2009**, *40*, 141–148. [[CrossRef](#)]
- Wu, Z.; Mirmiran, A.; Zhu, Z.; Swanson, J. Flexural behavior of prestressed FRP tubular bridge deck. *Compos. Part B* **2009**, *40*, 125–133. [[CrossRef](#)]
- Gautam, B.P.; Matsumoto, T. Shear deformation and interface behavior of concrete-filled CFRP box beams. *Compos. Struct.* **2009**, *89*, 20–27. [[CrossRef](#)]
- Kim, H.Y.; Park, K.T.; Jeong, J.; Lee, Y.H.; Hwang, Y.K.; Kim, D. A pultruded GFRP deck panel for temporary structures. *Compos. Struct.* **2009**, *91*, 20–30. [[CrossRef](#)]
- Chen, A.; Davalos, J.F. Strength evaluations of sinusoidal core for FRP sandwich bridge deck panels. *Compos. Struct.* **2010**, *92*, 1561–1573. [[CrossRef](#)]
- Li, Y.F.; Meda, H.A.; Chen, W. The Design and Analysis of Internally Stiffened GFRP Tubular Decks—A Sustainable Solution. *Sustainability* **2018**, *10*, 4538. [[CrossRef](#)]
- Hai, N.D.; Mutsuyoshi, H.; Asamoto, S.; Matsui, T. Structural behavior of hybrid FRP composite I-beam. *Constr. Build. Mater.* **2010**, *24*, 956–969. [[CrossRef](#)]
- Fam, A.; Honickman, H. Built-up hybrid composite box girders fabricated and tested in flexure. *Eng. Struct.* **2010**, *32*, 1028–1037. [[CrossRef](#)]
- Li, Y.F.; Hsu, T.H.; Hsieh, F.C. A Study on Improving the Mechanical Behaviors of the Pultruded GFRP Composite Material Members. *Sustainability* **2019**, *11*, 577. [[CrossRef](#)]
- Al-Kharat, M.; Rogers, C.A. Inelastic performance of cold-formed steel strap braced walls. *J. Constr. Steel Res.* **2007**, *63*, 60–474. [[CrossRef](#)]
- Ascione, F.; Feo, L.; Maceri, F. On the pin-bearing failure load of GFRP bolted laminates: An experimental analysis on the influence of bolt diameter. *Compos. Part B Eng.* **2010**, *41*, 482–490. [[CrossRef](#)]

20. Karakuzu, R.; Demircoren, O.; Icten, B.M.; Deniz, M.E. Failure behavior of quasi-isotropic laminates with three-pin loaded holes. *Mater. Des.* **2010**, *31*, 3029–3032. [[CrossRef](#)]
21. Jam, J.E.; Ghaziani, N.O. Numerical and experimental investigation of bolted joints. *Int. J. Eng. Sci. Technol.* **2011**, *3*, 285–296. [[CrossRef](#)]
22. Feo, L.; Mara, G.; Mosallam, A.S. Stress analysis of multi-bolted joints for FRP pultruded composite structures. *Compos. Struct.* **2012**, *94*, 3769–3780. [[CrossRef](#)]
23. Li, Y.F.; Jobe, O.; Yu, C.C.; Chiu, Y.T. Experiment and Analysis of Bolted GFRP Beam-Beam Connections. *Compos. Struct.* **2015**, *127*, 480–493. [[CrossRef](#)]
24. Olmedo, A.; Santiuste, C. On the prediction of bolted single-lap composite joints. *Compos. Struct.* **2012**, *94*, 2110–2117. [[CrossRef](#)]
25. Subramanian, C.; Senthilvelan, S. Effect of reinforced fiber length on the joint performance of thermoplastic leaf spring. *Mater. Des.* **2010**, *31*, 3733–3741. [[CrossRef](#)]
26. Smith, S.J.; Parsons, I.D.; Hjelmstad, K.D. Experimental comparisons of connections for GFRP pultruded frames. *J. Compos. Constr.* **1999**, *3*, 20–26. [[CrossRef](#)]
27. Lehman, D.; Roeder, C.; Herman, D.; Johnson, S.; Kotulka, B. Improved seismic performance of gusset plate connections. *J. Struct. Eng.* **2008**, *134*, 890–901. [[CrossRef](#)]
28. Kapti, S.; Sayman, O.; Ozen, M.; Benli, S. Experimental and numerical failure analysis of carbon/epoxy laminated composite joints under different conditions. *Mater. Des.* **2010**, *31*, 4933–4942. [[CrossRef](#)]
29. Davalos, J.F.; Salim, H.A.; Qiao, P.; Lopez-Anido, R. Analysis and design of pultruded FRP shapes under bending. *Compos. Part B Eng.* **1996**, *27*, 295–305. [[CrossRef](#)]
30. Masarira, A. The Effect of joints on the stability behaviour of steel frame beams. *J. Constr. Steel Res.* **2002**, *58*, 1375–1390. [[CrossRef](#)]
31. Hejll, A.; Taljsten, B.; Motavalli, M. Large scale hybrid FRP composite girders for use in bridge structures-theory, test and field application. *Compos. Part B Eng.* **2005**, *36*, 573–585. [[CrossRef](#)]
32. Li, Y.F.; Lin, Y.J.; Chen, C.W.; Lin, C.T. Theoretical and experimental studies on the as-built and repaired rehabilitated RC frames. *Can. J. Civ. Eng.* **2007**, *34*, 923–933. [[CrossRef](#)]
33. Gray, P.J.; McCarthy, C.T. A global bolted joint model for finite element analysis of load distributions in multi-bolt composite joints. *Compos. Part B Eng.* **2010**, *41*, 317–325. [[CrossRef](#)]
34. Balç, R.; Chira, A.; Chira, N. Finite element analysis of beam to column end plate bolted connection. *Civ. Eng. Arch.* **2012**, *55*, 24–29.
35. Computers and Structures Inc. *CSI Analysis Reference Manual for SAP2000. 2013 ETABS, SAFE and CSiBridge*; Computers and Structures Inc.: Berkeley, CA, USA, 2000.



© 2019 by the authors. Licensee MDPI, Basel, Switzerland. This article is an open access article distributed under the terms and conditions of the Creative Commons Attribution (CC BY) license (<http://creativecommons.org/licenses/by/4.0/>).